IDENTIFICATION OF ACTIVE PHASES IN PARTIAL OXIDATION CATALYSTS

A Dissertation

Submitted in partial fulfillment of the requirements
for the award of the degree of

MASTER OF SCIENCE

In

CHEMISTRY

by

Ulaganathan. R

Under the guidance of

Prof. B. Viswanathan

DEPARTMENT OF CHEMISTRY
INDIAN INSTITUTE OF TECHNOLOGY, MADRAS
CHENNAI – 600 036

APRIL 2008

CERTIFICATE

This is to certify that the project entitled **"IDENTIFICATION OF ACTIVE PHASES IN PARTIAL OXIDATION CATALYSTS"** is a bonafide work carried out by **Ulaganathan. R** in partial fulfillment of the requirements for the award of the degree of Master of Science in Chemistry at the Department of Chemistry, Indian Institute of Technology Madras (IITM).

Date: April , 2008

Place: IIT Madras

B. Viswanathan
Emeritus Professor, Chemistry
Department, I. I.T. Madras

ACKNOWLEDGEMENT

I express my sincere thanks and deep sense of gratitude to **Prof.B. Viswanathan**, my research guide for his constant encouragement, thought providing group discussions, unfailing guidance and creating scientific temperament at every stage of the research programme. I deem it a great privilege to be associated with him.

I would like to thank **Prof. R. Dhamodharan**, head of the department of chemistry for providing the necessary infrastructural facilities during my project tenure.

I would like to thank **Dr. B. Rajakumar**, for helping me in learning some aspects of theoretical chemistry.

I would like to thank seminar coordinators **Dr. Arti Dua** and **Dr. K.M. Muraleedharan**, for their help in organising my seminar.

I express my deep and special thanks to my co-guide **Dr. R. Mahalakshmy**, for her constant encouragement, support and guidance in all the aspects of my project.

I would like to express my special thanks to **T. M. Sankaranarayanan, Dr.B.Murugan, Mr. P. Indraneel, Dr. S. Sabiah, Mr. L. Himakumar, Mr. Ch.Venkateswara Rao, and Ms. M. Helen** with whom I have spent my memorable occasions in the lab and group discussions.

I thank my colleagues **Mr. B. Kuppan, Mr. N. Vamsikrishna, Mr.G. Ganesh, Mrs. S. Chandravadhanam, Mr. P. Ramanamurthy, Mr. K. Poliraju, K R. Suthager, Ms. P. Sangeetha, Ms. R. Sumathi, Ms. M. Banu, Mr. M. Navaladian, Mrs. C.M. Janet, Ms.T. Nithya and Mr. Jude Vimal Michael** and all other NCCR members for their help and deep encouragement.

I wish to thank **IIT Madras** for providing all the facilities to carry out the project work

My sincere thanks to all teaching and non teaching staffs of the department of chemistry, IIT madras.

I would also like to thank my parents and classmates for their long standing help and support.

I gratefully acknowledge computer centre **IIT Madras** for providing necessary facilities to carry out theoretical calculations.

ULAGANTHAN. R

ABSTRACT

Partial oxidation of hydrocarbon is an important areas of study. Bismuth molybdate and tin antimony oxides have been explored for their partia1 oxidising capability. Alpha phase of bismuth molybdate and antimony enriched surface of tin-antimony oxide were found to be the active phases. Moreover all the phases of bismuth molybdate catalysts differ only with respect to enrichments of molybdenum on the surface. There are various postulates regarding the surface enrichments and the resultant catalytic activity.

In the light of above, the present study aims at the identification of the active phase of these catalyst systems using computational methods. All the phases of bismuth molybdates and all the possible structures of tin antimony oxides have been modeled. The values of the energies and structural parameters like bond lengths have been compared to identify the active phase for partial oxidation.

TABLE OF CONTENTS

CHAPTER 1

INTRODUCTION

Tin antimony oxides and bismuth molybdates have been found to be good selective oxidation catalyst. The maximum catalytic activity was obtained with tin antimony oxide when the surface of the system was enriched with antimony. With respect to bismuth molybdates, α, β phases of bismuth molybdates have been found to be much more active than the γ phase. All these phases differ in the amounts of molybdenum segregation on the surface. α-phase with greater molybdenum segregation have been shown to be a much active catalyst compared to all other phases.

Computational methods prove to be a useful tool for determining the total energy of any system. The various other parameters like bond energy, surface energy along with HOMO and LUMO energies of the systems can be evaluated with the help of computational methods. There have also been significant advances in this field in recent developments of multiple alternate procedures like DFT and molecular mechanics. One can also locate global minimum of the molecule, by the process of geometry optimisation. Chemical reactions and its transition state can also be modelled. Of all the methods, DFT and molecular mechanics prove to be much useful for large electron systems, because of its lesser time scaling.

The present work features the computer modelling of the oxidation catalysts and identification of the active phase of the catalyst. This identification can be done by comparing the energies of catalyst in its reduced form and its parent structure. The oxidising power of the catalyst can be correlated with HOMO-LUMO energies. The energy of HOMO can be correlated with surface energy. Higher the surface energy, it

will be unfavourable for that surface to be formed. With the help of computational methods the active phases of partial oxidation catalysts viz., tin antimony oxide and bismuth molybdates have been studied in the present work.

CHAPTER 2

AN OVERVIEW OF COMPUTATIONAL CHEMISTRY

There are two broad areas in computational chemistry that are devoted to the determination of structure of molecule and reactivity viz., molecular mechanics and electronic structure theory.

The Role of Computational Chemistry

The methods consists of

- Computing the energy of the particular molecular structure (spatial arrangement of atom, nuclei or electron). Properties of the molecules in the computed energy state can also be predicted.
- Geometry optimisation, which leads to the geometry corresponding to the lowest energy state. It is the point at which first derivative of energy with respect to displacement is zero.
- Computing the vibrational frequencies of molecule resulting from inter atomic motions within the molecule. The frequency depends on the second derivative of energy with respect to displacement, (in other words Eigen values of the Hessian matrix are determined).

Locating the transition state structure, which locate the highest energy molecular structure relative to the specified starting structure. Any displacement at the point of transition state structure in the both the sides lead to decrease of energy.

2.1 Methods for Electronic Structure Theory

Electronic structure methods use the laws of Quantum mechanics to compute the energy and the other related properties of molecules. The energy can be calculated

through the laws of quantum mechanics, by Schrodinger wave equation. However, exact solution to Schrodinger equation is not computationally possible. Hence electronic structure methods are characterised by their various mathematical approximation and to generate the solution. There are two major classes of electronic structure methods.

- Semi-empirical methods, such as AM1, MINDO/3 and PM3, which use the parameter derived from the experimental data to simplify the computation.
- Ab-initio methods, unlike either molecular methods or semi-empirical methods, use no experimental parameters in the computations. The computations are based solely on the laws of Quantum mechanics (based on the first principle).

Ab-initio methods also depend on the values of the small number of physical constants like speed of light, the masses of the atoms consisting the molecule and charges of the electron and nucleus and Planck constant.

Semi-empirical and Ab-initio methods differ in computational cost and accuracy. Semi-empirical methods are relatively easier, less time consuming and provides reasonable qualitative description of molecular system. They also provide a good quantitative prediction of energy and structure for the system where good parameter sets exists.

The non-empirical method especially the conventional Hartree-Fock plus correlation space energy method is associated with sharp increase in the time requirement with increase in the size of basis set. For example, an N electron system contains 3N co-ordinates (three for each electron, four if spin is included). Hence the time scaling for

the conventional Ab-initio method is directly proportional to N^4 (or more depending upon the size of the system). Thus, the calculation of the electronic properties by conventional Ab-initio method is not feasible. Therefore, to solve the H-F equations, many approximations and assumptions have to be made that the electron interacts with average potential coming from other electrons. In reality, electronic correlation with their movement, try to avoid each other, so there is a least amount of electrostatic repulsion. In order to avoid these complexities and difficulties, Density Functional Theory (DFT) and Molecular mechanics are used to describe the many electron system.

2.2 Density Functional Theory

The basis of DFT is that ground state electronic energy is directly proportional to the electron density 'ρ'. In other words there exists one to one correspondence between electron density of the system and energy. The electron density can be expressed as a square of wavefunction integrated over N-1 electron co-ordinates. Hence this depends on the three co-ordinates independent of the number of electrons. The complexity of wave function increases with the increase in number of electrons, but density has same variable independent of the size of the system. Time scaling of DFT is directly proportional to N^3 (where N is the number of electrons of the system under consideration).

The DFT theory was born in 1964 with the publication of Hohenberg and Kohn. The main aspects of the theory are,

(i) Every observable of a stationary Quantum mechanical system including energy can be calculated in principle exactly from the ground state density.

(ii) Ground state density can be calculated in principle exactly using the variation method.

2.3 Kohn and Sham Method

Expression relating kinetic energy to density is not known accurately. The current expressions and even those improved upon the original Thomas-Fermi theory are crude and unsatisfactory. For that reason, Kohn and Sham opened the gateway for an ingenious method of merging wave function and density approach. They departition the total energy in the following parts

$$\mathbf{E[\rho] = To[\rho] + [Vext(r) + U_{el}(r)]\rho(r)\, dr + Exc\, \rho(r)}$$

The $T_0[\rho]$ is the kinetic energy of the electrons in a system which has the same density ρ as the real system, but in which there is no electron-electron interaction. This is frequently called a system of non interacting electron. But it may be understood, since electrons still interact with nuclei. U_{el} (r) is a pure Coulomb classical interaction between electrons. It includes electron self-interaction. Vext(r) is the external potential, i.e. from the nuclei. The last function Exc(ρ) is called exchange correlation energy. It includes all the energy contributions, which are not accounted for by previous terms. (i.e.)

(i) Electron exchange.

(ii) Electron correlation since non-interacting electrons do need to correlate their movements.

(iii) A portion of the kinetic energy which is needed to correct T_o (ρ) to obtain true kinetic energy of a real system T(ρ).

(iv) Correction for self-interaction introduced by the classical coulomb potential.

However, better approximations for this function are being available. Derivation of Kohn-Sham equations assumes energy function and under variational principle

$$\mu = \delta E[\rho(r)]/\delta\rho(r)=\delta T_o[\rho(r)]/\delta\rho(r)+Vext(r)+Uel(r)+\delta E_{xc}[\rho(r)]/\delta\rho(r)$$

$$\mu = \delta E[\rho(r)]/\delta\rho(r) = \delta T_o[\rho(r)]/\delta\rho(r)+ V_{eff}(r)$$

where all terms are lumped together, except noninteracting electron kinetic energy, into an effective potential depending upon r. The above equation calls for a Schrödinger wave equation in terms of density.

$$[-1/2\nabla i^2+V_{eff}(r)]\phi_i^{KS}(r) = \varepsilon_i\phi_i(r)^{KS}$$

This is similar to the eigen equation of the Hartree-Fock method, with one difference is the Fock operator in Hatree Fock Roothan method contains the potential, which is non local. i.e. different for each electron. The Kohn-Sham operator depends only on r, and not upon the index of the electron. It is the same for all electrons. The Kohn-Sham orbitals, which are quite easily derived from this equation, can be used immediately to compute the total density which can be used to calculate an improved potential V_{eff} (r) that can lead to a new cycle of self-consistent field. Density can also be used to calculate the total energy from equation in which the kinetic energy $T_o(\rho)$ is calculated from the corresponding orbitals, rather than density itself.

$$T_0(\rho) = 1/2\Sigma<\phi_i^{KS}|\nabla i^2|\phi_i^{KS}>$$

2.4 Molecular Mechanics

For calculation of ground state electronic properties of molecules, the geometry of a molecule should be at global minimum. The given geometry of a molecule should

correspond to a point at which the first derivative of energy with respect to displacement must be zero. Geometry optimisation of simple molecules like methane and water can be carried by quantum mechanical method. For a larger cluster of metal atoms (during modeling of a solid surface) the geometry optimization by quantum mechanical method is not reliable, because it will take four or five months to get required geometry for a given large electron system. In order to get an ideal geometry for large clusters, force field method is usually employed. In this force field method the molecules are modeled as atoms and held together by bonds. The molecule is described by a ball and spring model. Force field methods are also referred to as molecular mechanics methods. Molecular mechanics calculations do not explicitly treat the electrons in a molecular system. They perform computations based on the interactions among the nuclei. Electronic effects are implicitly included in the force fields through parameterisation. In addition to by passing the solution of the Schrodinger equation, quantum aspects of the nuclear motion are also neglected. This means that the dynamics of the atoms are treated by classical mechanics, i.e. Newton's second law.

The force field energy is written as the sum of the terms, each describing the energy required for distorting a molecule in a specific fashion.

$$\mathbf{E = E_{str} + E_{bend} + E_{tors} + E_{el} + E_{vdw} + E_{cross}}$$

$\mathbf{E_{str}}$ is the energy function for stretching bond between two atoms. $\mathbf{E_{bend}}$ represents the energy required for bending an angle; $\mathbf{E_{tors}}$ is the torsional energy for rotation around a bond. $\mathbf{E_{vdw}}$ and $\mathbf{E_{el}}$ **a**re describing the non-bonded atom-atom interactions and finally $\mathbf{E_{cross}}$ describes the coupling between the first three terms.

CHAPTER 3

COMPUTER MODELLING OF TIN ANTIMONY OXIDE

3.1 Introduction

$SnSbO_4$ acts as a good partial oxidation catalyst. It was found that selectivity for partial oxidation increased with increasing Sn/Sb ratio. It was also found that catalytic activity depends on the orientation and growth of the crystal planes and (100) plane expressed surfaces showed maximum activity. Hence, the questions regarding the phase identification along with the general features of the catalyst have been discussed.

In this work, our intention is to identify the active phase for the catalyst using computational methods**.** It has been shown that solid solution formation, formed by mixed tin and antimony oxides are limited to only a range of compositions of antimony. In most reports antimony compositions of about 3 at% Sb is soluble in tin dioxide. However, up to a max 6-7 at% Sb has also been reported [1, 2]. Higher Sb concentrations at the surface can be realised by heating at higher temperatures. Earlier studies indicate that antimony can be incorporated into tin dioxide lattice[3] upto a maximum concentration of 25 at% Sb. At all other compositions multiphase compositions were found to exist, consisting of rutile tin dioxide lattice and antimony oxide mainly Sb_2O_4 and Sb_6O_{13}[4]. The need for a prior knowledge with respect to formation of solid solutions and the oxidation state of ions, the nature of catalytic sites and the role of tin dioxide matrix have been discussed.

3.2 Solubility Limit of Antimony in Tin Dioxide Lattice

There appears to be a actual range in which a substitutional solid solution can exist. This is because Sb in +3 oxidation state cannot be incorporated in octahedral position in rutile phase. Lembarenskii et *al*[5] have concluded that solid solution of antimony in tindioxide is possible only upto 10 at% Sb. This is not in agreement with respect to x-ray studies of pyke *et al*. There was an increase in lattice parameters found with increasing concentration of antimony[6]. However, increasing antimony content above 5 at% had no effect on the values of lattice parameters.

3.3 Preparation

The tin antimony oxides were prepared by co-precipitating tin and antimony chlorides as their hydroxides and calcining them at wide range of temperatures between 650 -1150 °C. The preparation of the catalyst by the above method was found to be much more facile than by the direct solid state reaction. The solubility of antimony in tin dioxide is further confirmed by Mossbauer spectroscopy that is monitoring antimony (V) resonance. The ^{121}Sb Mossbauer spectroscopy showed the presence of antimony in Sb^{+5} and Sb^{+3} ions up to a maximum of 10 at% of Sb [7]. However, with respect to ^{119}Sn, Mossbauer parameters was found to be increasing with increasing antimony concentration, they do not show the presence of tin (II) ions. However, mixed tin and antimony oxides calcined at a temperature less than the volatalisation temperature of Sb_2O_4, gave signals for ^{121}Sb in +4 state, indicating the dominance of Sb_2O_4 phase. On the basis of the Mossbauer spectral data Berry agreed with the conclusions of Pyke *et al* [8] that calcination induces structural changes in an initially homogeneously precipitated material and leads to the segregation of excess antimony to the surface to form a separate Sb_2O_4 phase.

All these studies show that the solubility of antimony in tin dioxide is only up to a maximum of 5 at%. Moreover, Mossbauer spectra indicated that tin is present in +4 oxidation state and antimony is present as $(Sb^{+5})_{0.5}$ and $(Sb^{+3})_{0.5}$ ions. These antimony ions are octahedrally coordinated to oxygen in rutile like matrix of tin dioxide.

3.4 Active Sites in Mixed Tin and Antimony Oxides

There are various postulates regarding the active sites in tin and antimony oxides. The pure Sb_2O_4 phase is relatively inactive for the oxidation reaction[9]. The absence of reduction of tin (IV) and the observation of the presence of antimony (III) by means of Mossbauer spectroscopy[10] showed that easy oxygen loss is possible as a result of the reduction of antimony (V) ions to antimony (Ill) species. Since active catalysts are often calcined at high temperatures, it has been deduced that the antimony ions segregate and assume asymmetric sites surrounded entirely by tin (IV) cations in nearest-neighbour positions and that they are the active sites with acid-base properties required for the selective oxidation of olefins[10]. The acid and base sites of the catalyst surface, formed by neighbouring tin (IV) and antimony (III) species respectively, have been shown to be the sites for cyclic complex formation by proton rearrangement in the adsorption and isomerization of n-butenes[11]. The observed electron spin resonance signal at g ~ 1.89 is associated with electrons trapped in anionic vacancies, and these systems show high antimony (III) contents[12]. The observation that the yield of CO_2 decreased rapidly with decreasing tin concentration at the surface indicates that tin cations surrounded by other tin ions are favourable sites for the complete combustion reaction[13]. Although there is overwhelming evidence for the enrichment of antimony at the surface (this enrichment being a function of the antimony concentration as well as the calcination temperature), it appears that an active catalyst cannot contain a complete layer of Sb_2O_4 on the

surface. This is evident from the fact that Sb_2O_4 as such is inactive. These results have been taken to mean that surface antimony species which experience no direct or near-neighbour Sb-Sb interactions are the active sites. In this configuration it may mean that antimony ions surrounded by four or fewer tin ions alone can function as selective oxidation catalytic sites. There has been considerable doubt whether the matrix is the solid solution of antimony in tin (IV) oxide or pure tin oxide itself. But, however conclusive evidence is that basic site is formed by antimony, while the acidic sites are formed by tin ions. The possibility of localization and strong binding of electrons with antimony atoms available at the surface, rather than with tin ions might have been the thermodynamic driving force for Sb-Segregation [14].

3.5 Oxidation Mechanism of Tin and Antimony Oxides

Catalytic activity of mixed tin and antimony oxides was shown to be mainly due to remote control mechanism and spill over of oxygen. This was also confirmed by $^{18}O_2$ isotope studies[15]. Relaxation effect of antimony ions was also a major cause for catalyst's oxidizing capability. Antimony on the surface is highly coordinatively unsaturated and moreover it is in its highest oxidation state. Thus surface of the oxide is highly energetic and hence antimony has a high tendency to expand its coordination by bonding with bulk oxygen (relaxation effect), there by donating oxygen to the substrate. This has been proved by computational studies of mixed tin and antimony oxides by creation of oxygen vacancies in (100) plane.

3.6 Experiment

The (100) plane of mixed tin and antimony oxides has been pictorially represented in Figs.1and 2. In this figures red atom represents oxygen, violet atom represents antimony and green atom represents oxygen. These were called parent structures and

were subjected to geometry optimisation followed by energy calculation. After generating oxygen vacancy creation, the resulting structures were also subjected to geometry optimisation, followed by energy determination. These calculations were done using hybrid DFT/MM methods. Since, it is a large electron system; geometry optimisations were carried out using molecular mechanics and then energies were determined using DFT. Energies of systems with various oxygen vacancies structures were compared with that of the parent structures and feasibility of various structures for their oxidizing ability are discussed.

The structures are classified as bulk like and Sb-segregated. Bulks like structures are those in which Sb and Sn are alternating along the surface. Sb-segregated surface is the one in which there are only Sb atoms along the surface.

Parent structure of $SnSbO_4$

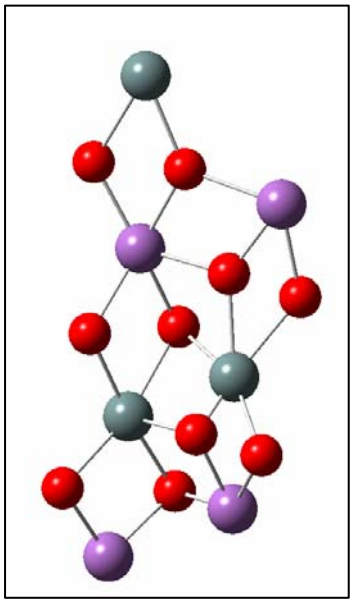

Fig.3.1. Bulk like

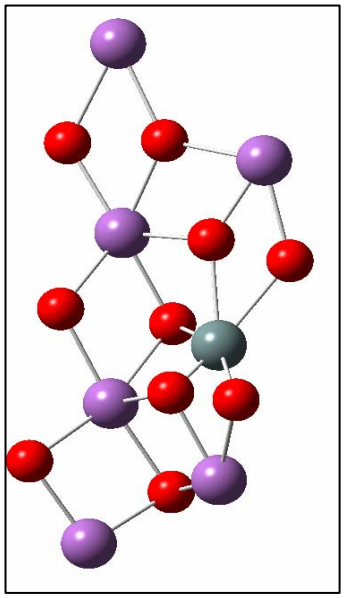

Fig.3.2. Sb-enriched surface

Table 3.1 Comparison of geometrical parameters obtained by theoretical calculation with that reported

Structural Parameters		Bond length	
		Theoretical	**Experimental**
Sn-O	In plane	2.105 Å	2.102 Å
	Bridging	2.118 Å	2.201 Å
Sb-O	In plane	1.98 Å	1.993 Å
	Bridging	1.97 Å	1.201 Å
Bond angle			
Sn-O-Sb	In plane	101.45°	102.1 °
	Bridging	102.5°	101.9 °
O-Sn-O	In plane	86.5°	84.9 °
	Bridging	87.0 °	85.4 °
O-Sb-O	In plane	88.1°	86.5 °
	bridging	87.05°	85.7 °

It has been shown that theoretically obtained values of lattice parameters match with those reported in literature. These results also indicate extent of accuracy that can be obtained in this lattice parameters values by using hybrid DFT/MM methods.

Table 3.2 Optimised geometrical data for the parent structure

Structural Parameters		Bond length	
		Input	**Output**
Sn-O	Inplane	2.08 Å	2.105 Å
	Bridging	2.00 Å	2.118 Å
Sb-O	Inplane	2.02 Å	1.98 Å
	Bridging	1.98 Å	1.97 Å
Bond angle			
Sn-O-Sb	Inplane	99.1°	101.45°
	Bridging	102.4°	102.5°
O-Sn-O	In plane	88.1°	86.5°
	Bridging	91.8°	87.0 °
O-Sb-O	Inplane	91.1°	88.1°
	bridging	91.7°	87.05°
Sb-O-Sb	Inplane	101.3°	101.3°
	Bridging	101.6°	101.5°

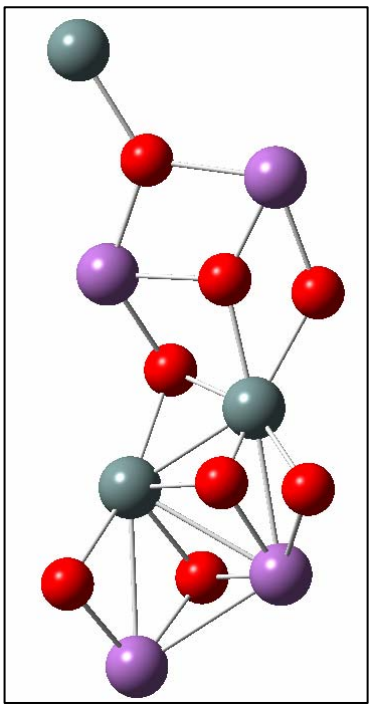

Fig. 3.3 1, 2 - Bulk like

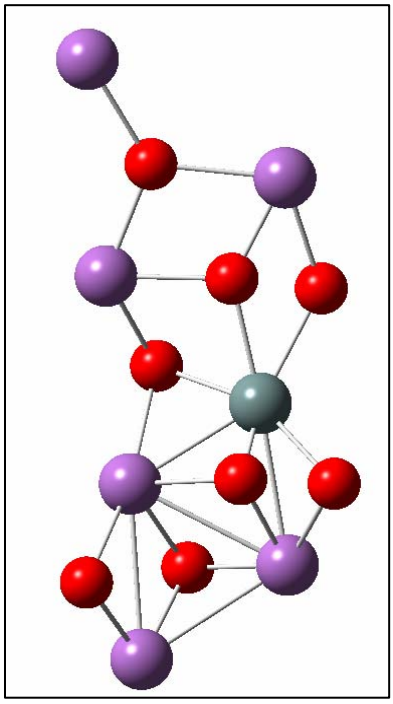

Fig. 3.4 1, 2- Sb enriched

Figures 3.3 and 3.4 are the optimised structures of 1,2- bulk like and 1,2-Sb-enriched. The values of their structural parameters are given in Table 3.3. Increase in the bond length and the contraction in the matrix were seen as a result of relaxation effect and lonepair-bondpair repulsions.

Table 3.3 Optimised geometric data for the 1, 2- bulk like

Structureal Parameter		Input	Output
		Bond length	
Sn-O	Inplane	2.08 Å	2.108 Å
	Bridging	2.0 Å	2.12 Å
Sb-O	Inplane	2.02 Å	2.01 Å
	Bridging	1.098Å	1.97 Å
		Bond angle	
Sn-O-Sb	Inplane	99.1°	99.8°
	Bridging	102.4°	100.1°
O-Sn-O	Inplane	88.1°	86.4°
	Bridging	91.8°	85.5°
O-Sb-O	Inplane	91.1°	85.91°
	Bridging	91.7°	86.10°

Table 3.4 Optimised geometric data for the 1, 2 Sb segregated

Structural Parameter		Input	Output
		Bond length	
Sn-O	Inplane	2.08 Å	2.111 Å
	Bridging	2.00 Å	2.125 Å
Sb-O	Inplane	2.02 Å	2.03 Å
	Bridging	1.09 Å	1.98 Å
		Bond angle	
Sb-O-Sb	Inplane	101.3°	99.5 °
	Bridging	101.6°	99.9 °
O-Sn-O	Inplane	88.1 °	85.87 °
	Bridging	91.8 °	85.3 °
O-Sb-O	Inplane	91.1 °	85.86 °
	Bridging	91.7 °	85.9 °

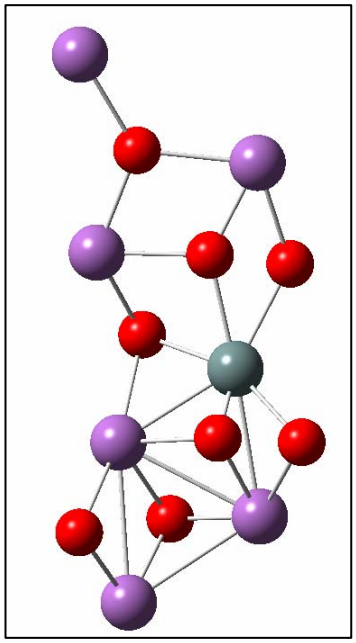

Fig.3.5 1, 3-bulk like

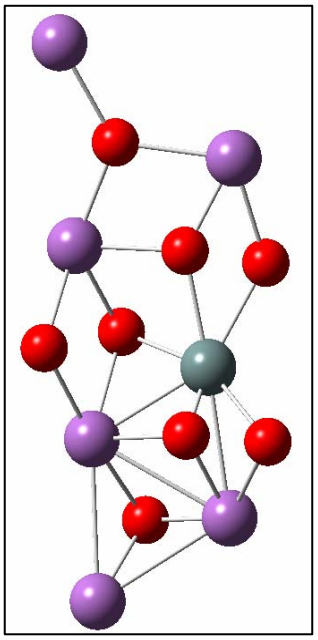

Fig. 3.6 1, 3-Sb-enriched

Figures 3.5 and 3.6 are the optimised structures of 1, 3- bulk like and 1, 3-Sb-enriched. The values of their structural parameters are given in Tables 3.5 and 3.6. Increase in the bond length and the contraction in the matrix have seen as a result of relaxation effect and lonepair-bondpair repulsions. 1,3-Sb-enriched surface was found to be much active compared to all other surfaces.

Table 3.5 Optimised data for 1,3-Bulk like

Structural Parameter		Input	Output
		Bond length	
Sn-O	Inplane	2.08 Å	2.115 Å
	Bridging	2.0 Å	2.129 Å
Sb-O	Inplane	2.02 Å	2.004 Å
	Bridging	1.98 Å	1.99 Å
		Bond angle	
Sn-O-Sb	Inplane	99.1 °	98.7 °
	Bridging	102.4 °	99.05 °
O-Sn-O	Inplane	88.1 °	86.7 °
	Bridging	91.8 °	85.11 °
O-Sb-O	Inplane	91.1 °	84.09 °
	Bridging	91.7 °	85.79 °

Table 3.6 Optimised data for 1,3-Sb-Segregated

Structural Parameter		Input	Output
		Bond length	
Sn-O	Inplane	2.08 Å	2.118 Å
	Bridging	2.0 Å	2.135 Å
Sb-O	Inplane	2.02 Å	2.06 Å
	Bridging	1.98 Å	2.01 Å
			Bond angle
Sb-O-Sb	Inplane	101.3°	98.3°
	Bridging	101.6°	98.7°
O-Sn-O	Inplane	88.1°	84.79°
	Bridging	91.8°	84.9°
O-Sb-O	Inplane	91.1°	84.35°
	Bridging	91.7°	84.8°

Table 3.7 HOMO-LUMO energy gap

Structure	HOMO (a.u.)	LUMO (a.u.)	Energy difference (HOMO - LUMO)
Bulk like	-0.1887	-0.1377	-0.051
Sb enriched	-0.1833	-0.1717	-0.0116

Higher HOMO-LUMO gap is seen for Sb-enriched surface, indicating its high oxidising capability.

3.7 Results and Discussion

The lone pair left after oxygen vacancy creation reduces Sb^{+5} to Sb^{+3} and is pointing towards the vacant site. As, a result of which there will be a lone pair-bond pair (lp-bp) repulsions, leading to an increase in bond lengths and there would also be a contraction effect of matrix due to relaxation. Creation of oxygen vacancy formation from its corresponding parent structure may lead to contraction of matrix and increase in bond length. Greater the contraction, greater will be the tendency to become more stable. Indirectly those structures tending to become more stable have a very high oxidising capacity.

The maximum increase in the bond length and the contraction in the bond angle were found to be in the 1, 3-Sb-enriched surfaces. In Table 3.7 HOMO-LUMO gap has been given. HOMO-LUMO gap was found to be much higher for this surface compared to all others, indicating its high oxidising capacity. This, higher activity was attributed to relaxation effect. The least activity from the data was shown by 1, 2-bulk like surface. This was attributed to absence of Sb-segregation. Moreover, creation of oxygen vacancy in the adjacent positions involves high energy and hence

energetically less feasible. All the other structures falls intermediate between the structure showing maximum and minimum activity. Therefore, the activity of the (100) phase in terms of enrichments of antimony on the surface have been clearly depicted.

3.8 Conclusion

It was found that feasibility for the formation of oxygen vacancy is more feasible for Sb-enriched surface compared to bulk like structures. This was attributed to relaxation effect of antimony ions. Formation of oxygen vacancy in the adjacent position is less feasible to any other structures. The (100) phase with a Sb-enriched surface has been found to be the active phase.

CHAPTER 4

COMPUTER MODELLING OF BISMUTH MOLYBDATE

4.1 Introduction

Bismuth molybdate has been reported to be a good partial oxidation catalyst. They can catalyse selective oxidation such as conversion of propene to acrolein etc[15]. About one quarter of organic compounds have been prepared using bismuth molybdate as catalyst. Its catalytic action was found to increase with increase in 'Mo' concentration on the surface. Moreover, bismuth molybdate crystallises in three different phases namely α, β, γ respectively. Maximum catalytic activity was obtained with this system when it is crystallised in α - phase. Hence, identification of the active surface phase has been done to compare the activities, using computational methods. All the three phases differ only with respect to Mo-enrichment on the surface.

4.2 Structural Details

Bismuth molybdate possesses fluorite like structure with the metal atoms occupying tetrahedral holes. Bismuth was found to be in $(Bi^{+3})_{0.5}$ and $(Bi^{+5})_{0.5}$ oxidation states, while molybdenum was found to be in +6 oxidation state.

4.3 Preparation

Bismuth molybdate catalysts have been prepared by mixing bismuth oxide and molybdenum oxide and calcining them at different temperatures for different phases. Calcining upto a temperature of 673K led to the formation of alpha phase with Bi/Mo ratio almost equal to 2/3[16]. Heating at a calcination temperature of 573K leads to the

formation of beta phase with Mo/Bi almost equal to 1[17]. While, calcining at higher temperature lead to the formation γ-phase[18].

Thus, in general the three phases can schematically be represented as,

- α PHASE = $(BOAOAOAO)_m$
- β PHASE = $(BOAOAO)_m$
- γ PHASE = $(BOAO)_m$

Where B, A, O represents alternative MoO_2^{2+} (A) layers, $Bi_2O_2^{2+}$ (B) layers and O_2^{2-} (O) layers.

4.4 Oxidation Mechanism

Partial oxidation of bismuth molybdate follows a similar mechanism as has been observed with tin antimony oxides. They exert their catalytic activity by remote control mechanism and spill over of oxygen. This has been confirmed by $^{18}O_2$ isotopic studies. Moreover molybdenum present along the surface in the highest +6 oxidation state. Hence, it helps the catalyst to exert its activity by relaxation effect. This relaxation effect allows molybdenum to increase its coordination number by interacting with the bulk.

4.5 Nature of Acid-Base Sites

The presence of acidic and basic sites are responsible for catalytic activity. These sites must be of optimum strength. Using hard-soft acid-base theory 'Bi' centre constitutes an acid site, while Mo centre constitutes a basic site. According to Burrington et al.[19], active sites for propylene chemisorption are molybdenum dioxo groups bridged to bismuth–oxygen groups while the oxygen atoms bridged to Bi(III) sites are utilised by α hydrogen atoms of propylene. The presence of molybdenum

dioxo group and Bi(+3) oxidation state were found to be much high for alpha, followed for beta and gamma phases in the decreasing order.

4.6 Experiment

The alpha, beta, gamma phases have been modelled. Oxygen vacancies in the position (1, 3) have been created in each of the phases and the corresponding data such as energy, HOMO-LUMO gap and various other structural parameters like bond lengths have been computed. Optimisation of all the structures has been carried out with molecular mechanics and their energies are evaluated using DFT. The parent structures of bismuth molybdate for all the phases are represented in Fig 4.1. The violet balls represent bismuth, green balls represent molybdenum and red balls represent oxygen. After generation of oxygen vacancy the structures are compared with parent structures and its oxidising capability have been discussed. Moreover, HOMO-LUMO gap and various other structural parameters are also compared.

Fig. 4.1 Parent structures of Bismuth molybdate

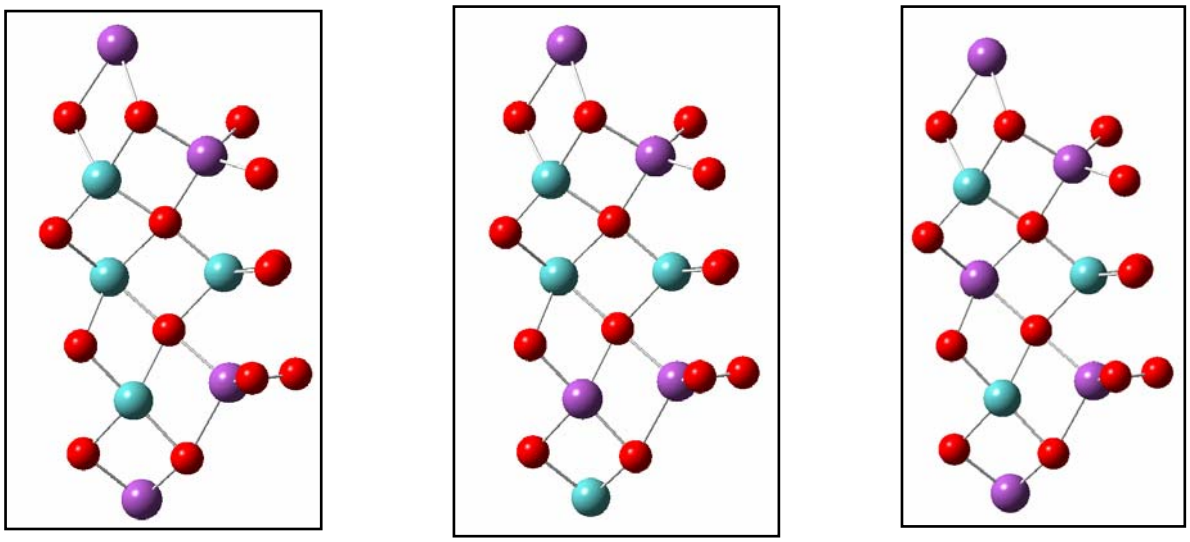

(a) **(b)** **(c)**

(a) α - Phase (b) β-Phase (c) γ-Phase

Fig. 4.2 Optimised parent structures of bismuth molybdate

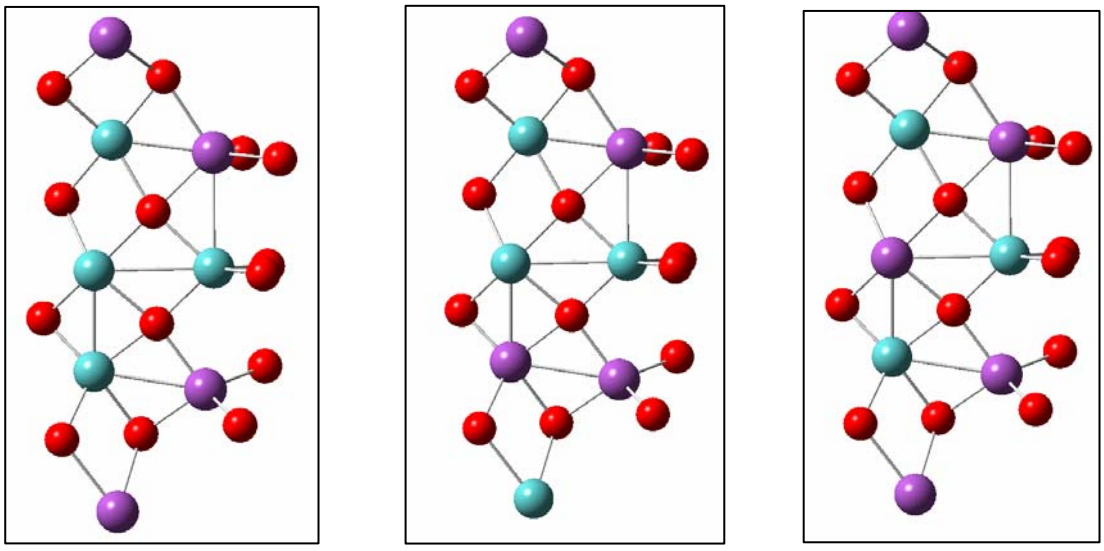

(a) α - Phase (b) β-Phase (c) γ-Phase

Fig. 4.3 Optimised 1,3-O-vacant bismuth molybdates.

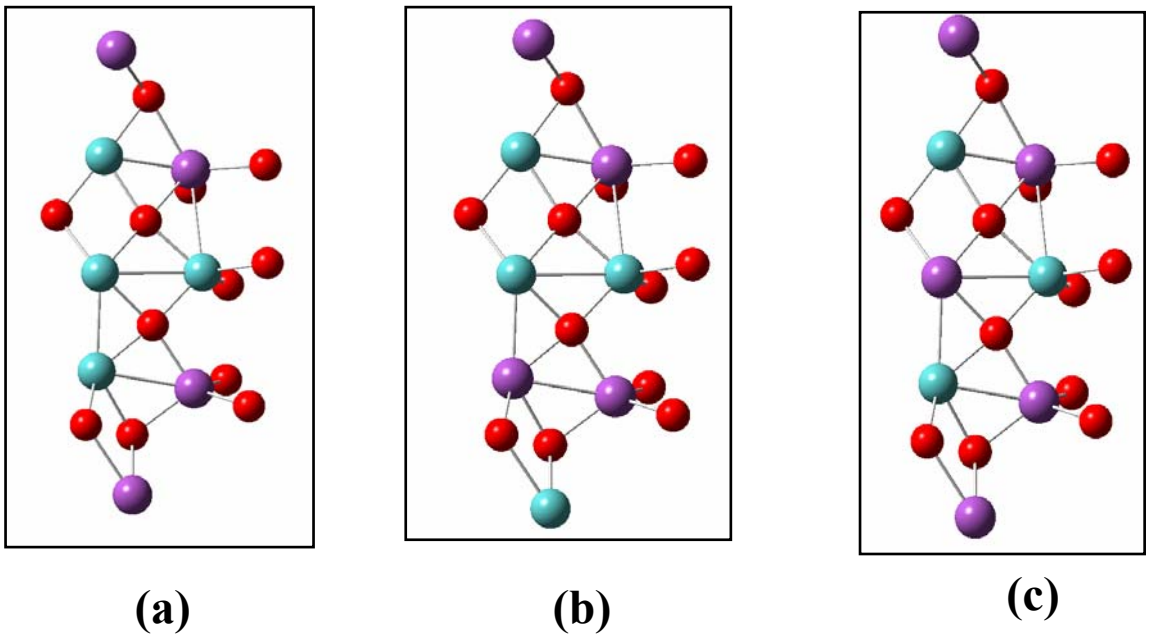

(a) α - Phase (b) β-Phase (c) γ-Phase

Table 4.1 Optimised geometric data for the parent structures

Structural parameters		Input	Output
		Bond length	
Bi-O	In plane	2.20 Å	2.15 Å
	Bridging	2.00 Å	2.345Å
Mo-O	In plane	1.98 Å	1.95 Å
	Bridging	1.94 Å	1.89 Å
		Bond angle	
Bi-O-Mo	In plane	84.5°	83.0°
	Bridging	89.9°	87.0°
O-Bi-O	In plane	109.0°	103.0°
	Bridging	109.0°	107.0°
O-Mo-O	In plane	109.0°	107.5°
	Bridging	109.0°	108.0°
Mo-O-Bi	In plane	88.0°	86.0°
	Bridging	87.0°	86.5°

Table 4.2 Optimised geometric data for the 1, 3-α-Bismuth molybdate

Structural parameters		Input	Output
		Bond length	
Bi-O	In plane	2.2 Å	2.31 Å
	Bridging	2.0 Å	2.56 Å
Mo-O	In plane	1.98 Å	2.02 Å
	Bridging	1.94 Å	1.97 Å
		Bond angle	
Bi-O-Mo	In plane	84.5°	80.5 °
	Bridging	89.9 °	87.2 °
O-Bi-O	In plane	109.0 °	101.2 °
	Bridging	109.0 °	103.5 °
O-Mo-O	In plane	109.0 °	105.3°
	Bridging	109.0°	107.9 °
Mo-O-Mo	In plane	88.0 °	85.8°
	Bridging	87.0°	84.5 °

Table 4.3 Optimised geometric data for the 1, 3-β-bismuth molybdate

Structural parameters		Input	Output
		Bond length	
Bi-O	In plane	2.2 Å	2.25 Å
	Bridging	2.0 Å	2.44 Å
Mo-O	In plane	1.98 Å	1.99 Å
	Bridging	1.94 Å	1.95 Å
Bond angle			
Bi-O-Mo	In plane	84.5°	82.5 °
	Bridging	89.9 °	85.6 °
O-Bi-O	In plane	109.0 °	103.3 °
	Bridging	109.0 °	105.5 °
O-Mo-O	In plane	109.0 °	107.3°
	Bridging	109.0°	108.0 °
Mo-O-Mo	In plane	88.0 °	86.2°
	Bridging	87.0°	86.5 °

Table 4.4 Optimised geometric data for the 1,3-γ-Bismuth Molybdate

Structural parameters		Input	Output
Bond length			
Bi-O	In plane	2.2 Å	2.241 Å
	Bridging	2.0 Å	2.365 Å
Mo-O	In plane	1.98 Å	2.02 Å
	Bridging	1.94 Å	1.99 Å
Bond angle			
Bi-O-Mo	In plane	84.5°	82.6 °
	Bridging	89.9 °	86.1 °
O-Bi-O	In plane	109.0 °	103.0 °
	Bridging	109.0 °	105.2 °
O-Mo-O	In plane	109.0 °	107.5°
	Bridging	109.0°	106.8°

Table 4.5 HOMO-LUMO energy gap

Structure	HOMO (a.u.)	LUMO (a.u.)	Energy difference (HOMO - LUMO)
□̃ Phase	-0.2655	-0.2583	-0.072
□̃ Phase	-0.2466	-0.2635	-0.101
γ - Phase	-0.2765	-0.2534	-0.231

4.7 Results and Discussions

The two electrons left after vacancy creation reduces Mo^{+6} to Mo^{+4} with the lone pair of electrons pointing towards the vacant site. Creation of oxygen vacancy leads to an increase in bond length and contraction of matrix, due to lone pair- bond pair repulsions. The structure, in which there is maximum increase in the bond length and maximum contraction of its matrix, will have a higher activity. In Table 4.5 HOMO-LUMO energy gap has been given. The structure that posses higher HOMO-LUMO gap, has a very high oxidising ability. It was found that α phase possesses higher catalytic activity compared to β and γ phases. Its HOMO-LUMO gap was found to be higher compared to all other phases, with 1,3-O vacancy formation dominating other structures. The data of structural parameters obtained from literature do not match with theoretically compared data. This could be due to the fact that coordination number of molybdenum was six, but in the model it has been assumed to be four for the computational convenience.

4.8 Conclusion

It was found that alpha phase of bismuth molybdate was active since the HOMO-LUMO gap was found to be higher for alpha phase compared to all other phases.

5. References

1. F.J. Berry, *Adv. Catal., 30* (1981) 97.
2. K. Wakabayashi, Y. Kamiya and N. Ohta, *Bull. Chem. Soc. Jpn., 40* (1967) 2172.
3. F.J. Berry, *J. Catal., 73* (1982) 349.
4. Y. M. Cross and D. R. Pyke, J. *Catal., 58* (1979) 61.
5. R. A. Lemberanskii, I. B. Annenkova and E. S. Liberman, *Zh. Fiz. Khim., 56* (1982),1133.
6. D. R. Pyke, R. Reid and J. D. Tilley, J. *Chem. Soc., Faraday Trans. I,* 76 (1980)1174.
7. Yu. E. Roginskaya, D. A. Dulin, S. S. Stroeva, N. V. Kulkova and A. I. Gelbshtein,*Kinet. Catal., 9* (1968) 943.
8. F. Sala and F. Trifiro, *Z. Phys. Chem. N.F., 95* (1975) 279.
9. Y. Boudeville, F. Figueras, M. Forissier, J. L. Portefaix and J, C. Vedrine, *J. Catal., 58* (1979) 52.
10. J. C. McAteer, J. *Chem. Soc., Faraday Trans. I, 75* (1979) 2762.
11. B. Naggy, A. Abou-Kais, M. Guelton, J. Harmel and E. G. Derouane, *J. Catal., 73* (1982) 1.
12. F.J. Berry and J. C. McAteer, *Inorg. Chim. Acta, 50* (1981) 85.
13. J, C. McAteer, *J. Chem. Soc., Faraday Trans. L 75* (1979) 2768.
14. P. A. Cox, R. G. Egdell, C. Harding, W. R. Patterson and P. J. Tavener, *Surf. Sci., 123* (1982) 179.
15. R.K. Grasselli. *Catal. Today 49* (1999) 141.
16. Ph.A. Batist, J.F.H. Bouwens and G.C.A. Schuit. *J. Catal. 25* (1972) 1.

17. F. Trifiro, H. Hoser and R.D. Scarle. *J. Catal. 25* (1972) 12.

18. B. Grzybowska, J. Haber and J. Komorek. *J. Catal. 25* (1972) 25.

19. J.D. Burrington, C.T. Kartisek and R.K. Grasselli. *J.Catal. 81* (1983) 489.